HIGH-EFFICIENCY AMORPHOUS SILICON AND NANOCRYSTALLINE SILICON BASED SOLAR CELLS AND MODULES

Quarterly Technical Progress Report
February 1 through April 30, 2007

S. Guha and J. Yang
United Solar Ovonic LLC
Troy, Michigan

NREL Technical Monitor: Bolko von Roedern

Prepared under Subcontract No. ZXL-6-44205-14

Table of Contents

Preface

This Quarterly Report covers the work performed by United Solar Ovonic LLC under the Thin Film Partnership Subcontract No. ZXL-6-44205-14 for the period from February 1, 2007 to April 30, 2007. The following personnel participated in this research program.

A. Banerjee, E. Chen, S. Guha (Principal Investigator), B. Hang, M. Hopson, J. Noch, J. M. Owens, T. Palmer, L. M. Sivec, D. Wolf, X. Xu, B. Yan, J. Yang (Co-Principal Investigator), K. Younan, and G. Yue .

Collaboration with National Renewable Energy Laboratory is greatly acknowledged.

Executive Summary

We have worked on many areas of improving the a-Si:H, a-SiGe:H, and nc-Si:H based multi-junction solar cell efficiency and optimized the different elements of the mutli-junction solar cells. The major focuses were high rate deposition of nc-Si:H solar cells with MVHF glow discharge and large-area uniformity deposition of nc-Si:H solar cells. We have carried out the optimization of different hydrogen dilution profiles and tried to correlate the deposition process with material properties and solar cell performance. The characterization work has been carried out at the University of Oregon and NREL. However, the full characterization has not been finished. We will report the results when it is complete.

We have worked on the optimization of Ag/ZnO. Through the collaboration with NREL, we have systematically characterized the Ag/ZnO structures and correlated the surface roughness to solar cell performance.

We have studied the electrical bias effect on the stability of a-Si:H/nc-Si:H double-junction solar cells. We found that the a-Si:H/nc-Si:H double-junction solar cells with a bottom cell limited current mismatch showed a higher light-induced degradation under the short-circuit condition than the open circuit condition. This observation is consistent with the previously observed bias dependence of light-induced degradation in nc-Si:H single-junction cells.

We have worked on the large-area nc-Si:H solar cells and tried to improve the uniformity and efficiency. Based on the manufacturing requirements, we have worked on the nc-Si:H deposition using a moderate spacing between the cathode and the substrate to reduce the complicity of manufacturing machine design. Currently, we have achieved a module efficiency similar to that made with a smaller gap spacing.

1. Optimization of Ag/ZnO back reflector

1. 1. Introduction

High efficiency thin film solar cells need not only high quality active semiconductor layers, but also inactive contact layers such as top transparent contact and bottom contact. In United Solar, high efficiency hydrogenated amorphous silicon (a-Si:H) and silicon germanium (a-SiGe:H) alloys, and nanocrystalline silicon (nc-Si:H) solar cells are deposited on Al/ZnO or Ag/ZnO back reflector coated stainless steel substrates. The function of the metal coating is to reflect the light reaching the substrate, and the ZnO enhances the scattering of light through increased surface texture. United Solar's back reflectors have been developed since the late 80s and early 90s [1]. We have successfully implemented the optimized back reflectors in several roll-to-roll manufacturing lines. In the recent years, nc-Si:H based solar cells have gradually dominated in the research and development of high efficiency silicon based thin film solar cells because of the higher current density and better stability than the a-Si:H and a-SiGe:H cells. The multi-junction solar cells with a-Si:H in the top cell and nc-Si:H bottom cell promise higher efficiencies than the conventional a-Si:H/a-SiGe:H/a-SiGe:H triple-junction structure. We have achieved an initial and stable active-area efficiency of 15.1% and 13.3%, respectively, using the a-Si:H/a-SiGe:H/nc-Si:H and a-Si:H/nc-Si:H/nc-Si:H triple-junction solar cells [2, 3]. These results have surpassed the records achieved using the conventional a-Si:H/a-SiGe:H/a-SiGe:H triple-junction structure [4]. The high efficiency was partially due to an improved back reflector with more effective light trapping [5]. In order to achieve even higher efficiency, we need to improve the light trapping effect further. In this quarter, we have systematically optimized the Ag and ZnO deposition process and correlated the deposition parameters to the material properties and the solar cell performance.

1. 2. Experimental details

Ag/ZnO back reflectors were deposited in a batch machine with sputtering under different conditions. Two types of Ag layers were used: a textured Ag layer similar to our conventional Ag/ZnO and a flat, specular Ag layer for reducing the parasitical loss at the Ag/ZnO interface. Different ZnO thicknesses were used for increasing the texture. The material structures were measured at NREL using X-ray diffraction (XRD) and atomic force microscopy (AFM).

We deposited a-SiGe:H single-junction solar cells using a multi-chamber glow discharge system on different back reflectors. Current density versus voltage (J-V) characteristics were measured under an AM1.5 solar simulator and quantum efficiency (QE) curves were measured under the short circuit condition.

1. 3. Results and discussion

1.3.1. XRD analysis

Twelve Ag/ZnO back reflector coated stainless steel substrates were characterized at NREL by Chun-Sheng Jiang. Table I lists the sample structural properties. One

Table I. Ag/ZnO structural properties.

Sample ID	ZnO thickness (μm)	ZnO Ts	Ag state
R1938	0.8	High	Textured
R8272	0.5	Low	Textured
R8273	1.1	Low	Textured
R8283	1.5	Low	Textured
R8286	2.0	Low	Textured
R8322	3.0	Low	Textured
R8289	0.5	Low	Flat
R8290	1.0	Low	Flat
R8306	1.5	Low	Flat
R8314	2.0	Low	Flat
R8316	3.0	Low	Flat
R8342	2.0	High	Textured

sample (R1938) from the 5MW roll-to-roll production machine was used as a baseline reference. Five samples were made with different thicknesses of low temperature ZnO on a textured Ag layer and another five samples were made with different thicknesses of low temperature ZnO on a flat Ag layer. The last one was with 2-μm-thick high temperature deposited ZnO on flat Ag. The XRD spectra were measured on all of the samples with an X-ray from the K_α radiation from a copper anode. Figure 1 shows the XRD spectra of the baseline sample R1938. From the plot in a wide range (Fig. 1 (a)), eight peaks were observed with the following identifications: ZnO (002) at 34.28˚, Ag (111) at 38.22˚, Ag (200) at 44.54˚, ZnO (103) at 62.74˚, Ag (220) at 65.28˚, un-identified 72.40˚, Ag (113) at 77.66˚, and un-identified 82.14˚. It appears that the ZnO layer has a strong (002) preferential orientation and Ag layer with (111) preferential orientation. Since the two preferential peaks are much stronger than other peaks, we only use these two for analysis. First, we did grain size analysis. We used the Scherrer formula:

$$d = \frac{0.9\lambda}{\Delta\theta \times \sin(\theta)} \ , \tag{1}$$

to estimate the grain size, where λ is the X-ray wavelength (0.15428 nm), Δθ is the full width at the half maximum, and θ the peak position. Figure 2 (a) plots the Ag and ZnO grain sizes obtained from the Ag (111) and ZnO (002) peaks with different ZnO thicknesses, respectively. We found that there is no clear trend that the grain size changes with the ZnO thickness for both the Ag and ZnO layers. It is easy to understand that the Ag grain size does not change with the ZnO thickness because the same Ag layer was used for the given series of samples. However, a similar grain size for the textured Ag and flat Ag layers is unexpected because the flat Ag should have a smaller grain size. Detailed investigations, including the thermal induced crystalline changes, are necessary to find the mechanism. The ZnO grain size is in the range of 17 to 25 nm without a clear trend of increase with ZnO thickness. This could be explained by the zone growth model [6,7]. In certain conditions, the grains grow in columnar shape, where the lateral size does not increase with film thickness. Figure 2 (b) plots the XRD signal ratio

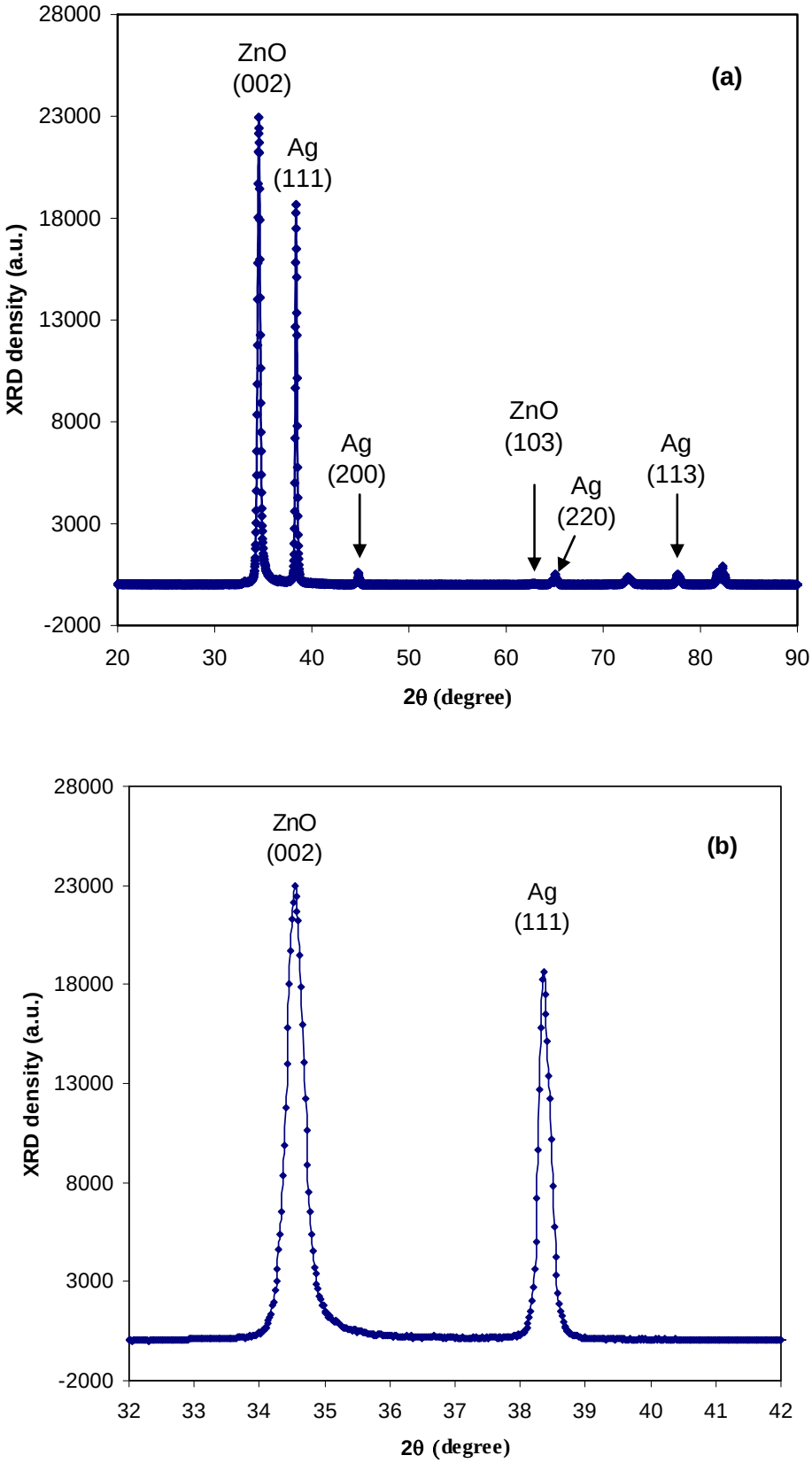

Figure 1. XRD spectra of R1938 (a) in a wide range and (b) in a narrow range.

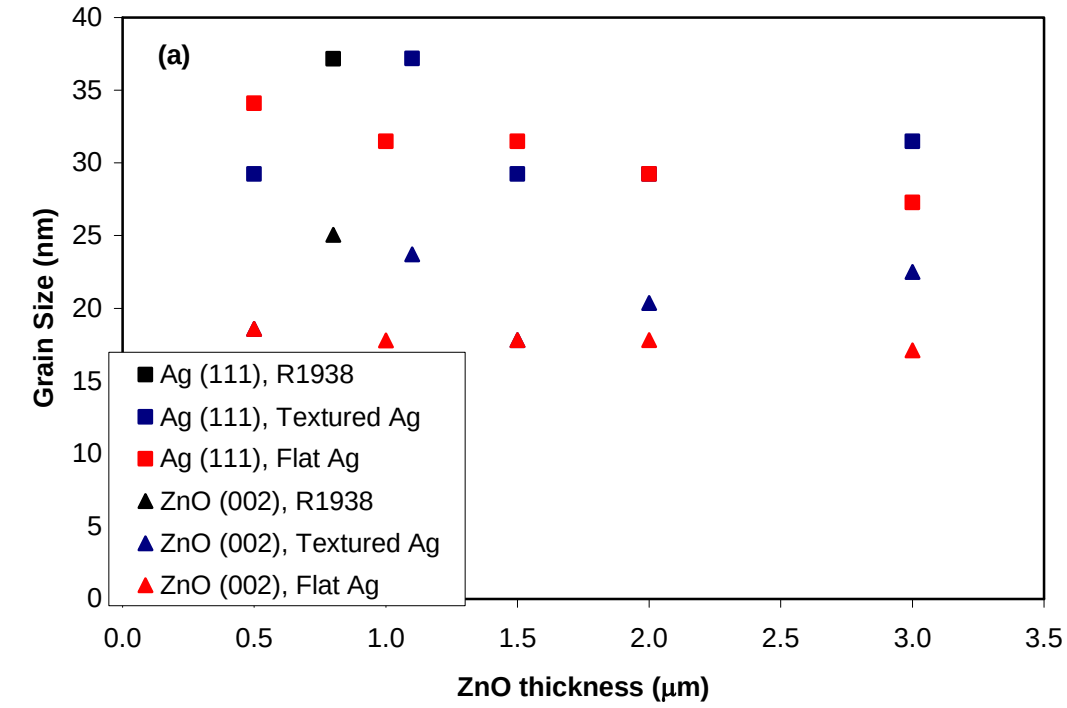

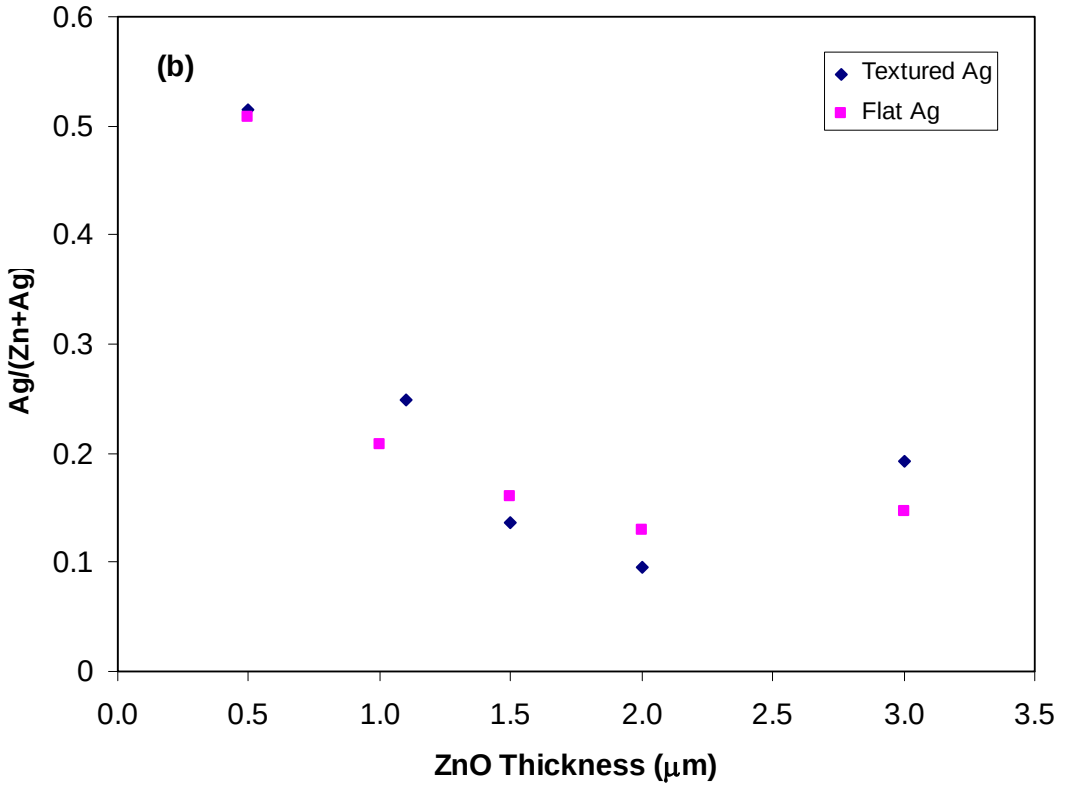

Figure 2. (a) Ag (111) and ZnO (002) grain sizes and (b) the XRD intensity ratio of Ag (111) and ZnO (002) as a function of ZnO thickness.

of the Ag (111) and ZnO (002). The results show that the relative Ag signal is reduced by the increased thickness of the ZnO layer except for the samples with a 3-μm-thick ZnO layer.

1.3.2. Surface morphology analysis with AFM measurements

The twelve Ag/ZnO back reflectors were also measured using AFM for surface roughness analysis. Figure 3 plots AFM images of different samples. The top left image was taken from R8289 with flat Ag and a 0.5-μm-thick ZnO layer deposited at a lower temperature, where fine sharp features appear. The top right one was from R8272 with a textured Ag with a 0.5-μm-thick ZnO deposited at the lower temperature, where the feature size becomes large and the feature shape becomes more rounded than the one on flat Ag. The lower left one was from R8342 with flat Ag/ZnO and a 2-μm-thick ZnO layer deposited at the higher temperature. The features in this picture are much larger than those on the top two samples and the feature shape becomes cratered. The lower right one was from the baseline sample of R1938, where both the Ag and ZnO were textured. The lateral sizes of the features are much larger in this sample and some larger plateaus appear with many crater shape features similar to sample R8342. Figure 4 plots the RMS roughness versus the ZnO thickness. For the series of samples with flat Ag, the RMS roughness linearly increases with ZnO thickness from 0.5 to 2 μm and then levels off. The RMS roughness of the samples on textured Ag shows an initial roughness from the textured Ag layer, increases in the range up to 2.0 μm, and levels off for samples with even thicker ZnO layer. If the RMS roughness is a critical parameter for light trapping in solar cells, a 2-μm-thick thick ZnO probably is the optimal thickness for the back reflectors. There are two extra samples on the plot. The baseline sample R1938 with a textured Ag and high temperature ZnO. It shows an enhanced RMS roughness. Similarly, the ZnO in R8342 was also deposited at higher temperature than the two series samples and showed a larger RMS roughness.

The RMS roughness only shows the vertical changes of the surface morphology. However, the lateral scale of the textured features is also important for light trapping in solar cells. There are two methods for the lateral size representation. The first is the autocovariance function, which is calculated by the following equation,

$$c(x, y) = \langle [h(x, y)h(x + \Delta x, y + \Delta y)] \rangle , \quad (2)$$

Where $h(x,y)$ is the surface height at position (x,y) and $\langle \quad \rangle$ means an average over the entire surface for Δx and Δy. Figure 5 shows (upper picture) the plot of the two dimensional autocovariance function and (lower picture) the map of correlation length of sample R8342, where the correlation length is the distance from the center of the half circle to the point where the color changes from dark blue to white. The mathematical definition of the correlation length is the distance over which the correlation function along a given direction decreases by a factor of 1/e=0.37. The scattering of the correlation length in the half circle represents the variation in different directions from the center of the AFM pictures. The important parameter is the minimum correlation length, which is the minimum value of the correlation length in all the directions. The minimum correlation length represents the lateral feature size on a rough surface. Figure 6 plots the minimum correlation length as a function of ZnO layer thickness. It shows that the lateral size increases with the ZnO thickness. The initial lateral size is smaller on

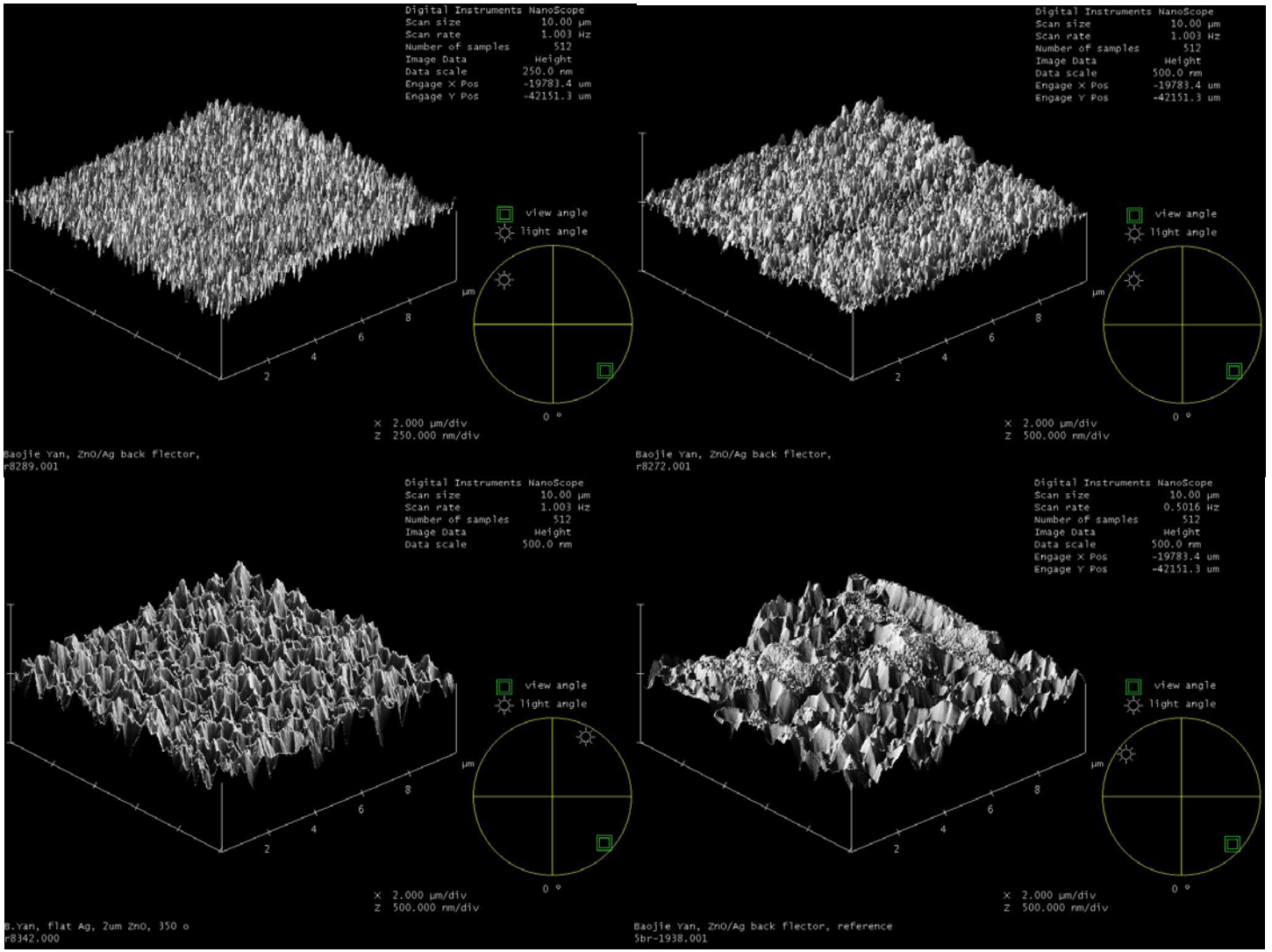

Figure 3. AFM images of Ag/ZnO back reflectors of R8289, R8272, R8342, and R1938 as listed in Table I.

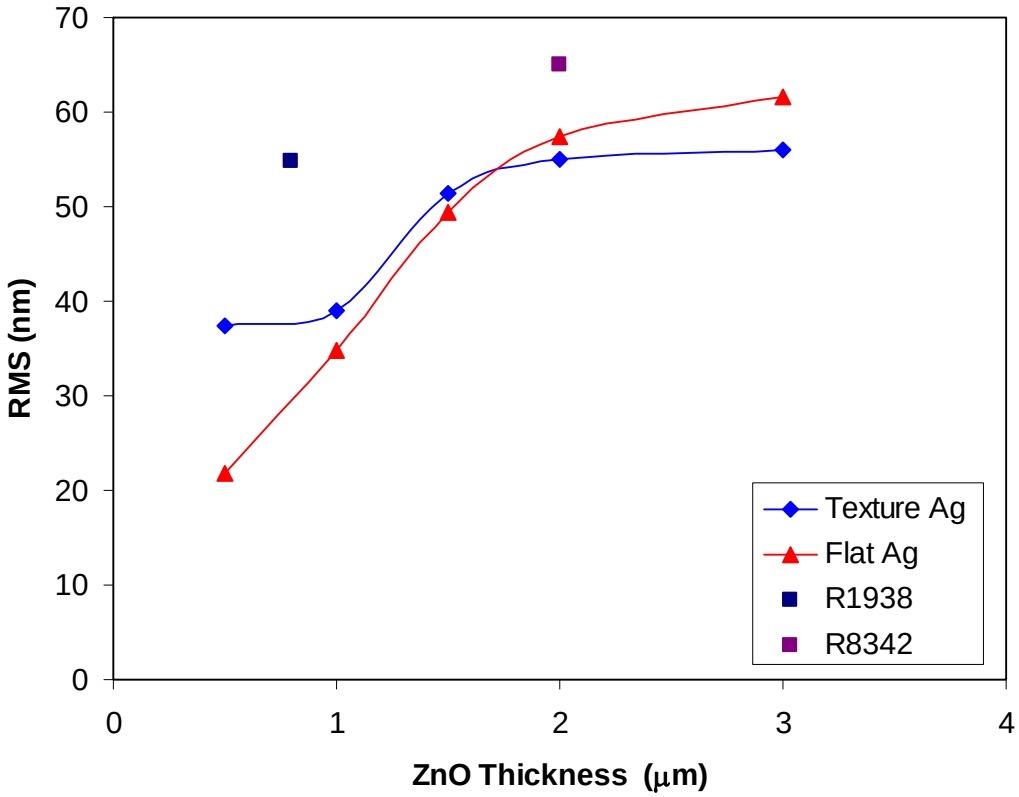

Figure 4. RMS roughness as a function of ZnO layer thickness in Ag/ZnO back reflectors.

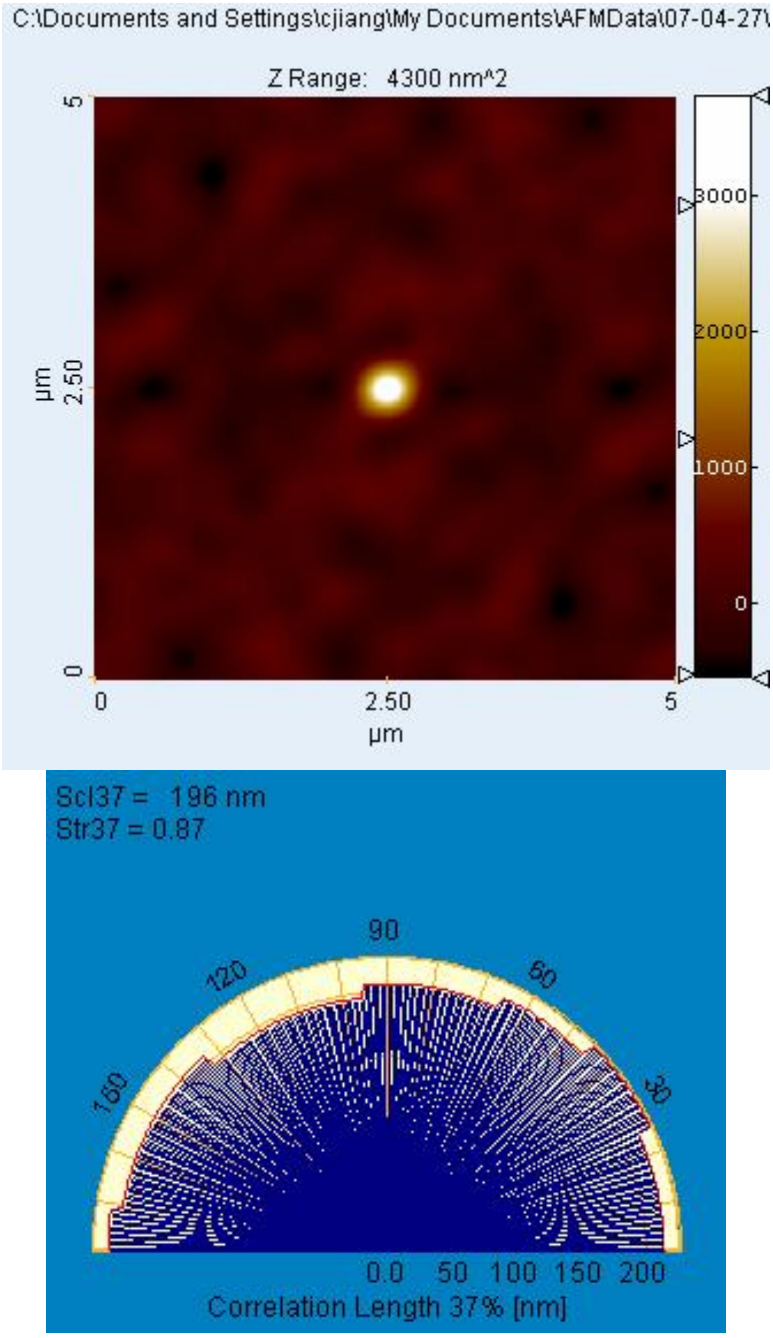

Figure 5. The upper picture is a two dimensional autocovariance function, and the lower one is the correlation length plot on a half circle.

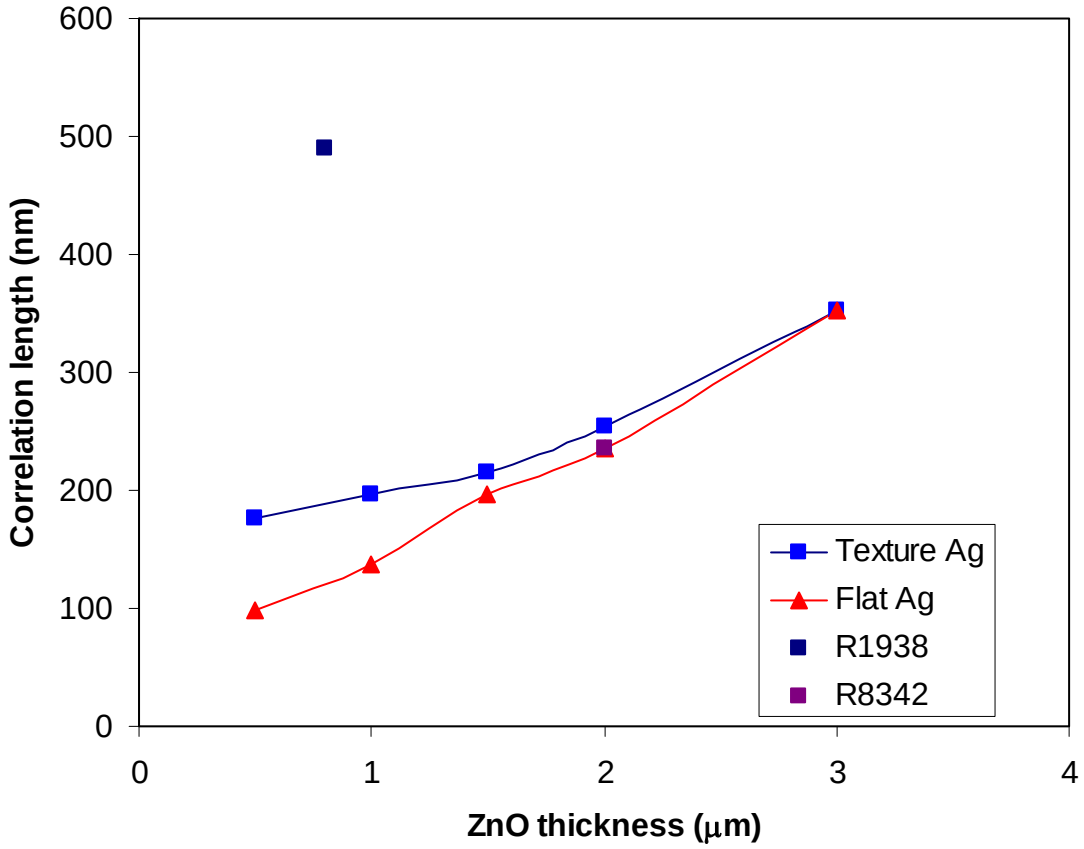

Figure 6. Minimum correlation length of Ag/ZnO back reflector versus the thickness of the ZnO layer.

the samples with a flat Ag layer than with a textured Ag layer because the textured Ag also contributes to the feature size. The lateral size continually increases with the ZnO layer thickness without the tendency of saturation as shown in the the RMS plots in Fig. 4. The minimum correlation length of sample R1938 is much larger than the other samples, which is consistent with the direct appearance in the picture of Fig. 3, where large plateaus are in a length over micrometers.

To summarize the observations, we found that both the vertical and lateral sizes of micro-features on the Ag/ZnO back reflectors increases with the ZnO thickness although there is no clear indication of ZnO grain size increase with thickness. The vertical roughness saturates when the ZnO thickness is over 2 μm, but the lateral size does not show the saturation trend. It may imply that the slope of the micro-features decreases with the ZnO thickness. Because the grain sizes estimated from XRD are much smaller than the lateral feature sizes, we would suspect that one micro-feature contains many grains. Therefore, although the grain size does not increase with the ZnO thickness, the texture does.

1.3.3. a-SiGe:H solar cells on optimized Ag/ZnO back reflectors

We have made two types of a-SiGe:H single-junction solar cells using slow rate RF glow discharge deposition on different Ag/ZnO back reflectors. The medium bandgap cells with an open-circuit voltage (V_{oc}) around 0.75 V under the AM1.5 illumination and low bandgap cells with an AM1.5 V_{oc} around 0.65 V are normally used for the middle and bottom cells in the a-Si:H/a-SiGe:H/a-SiGe:H triple-junction structure. The current versus voltage (J-V) characteristics of the solar cells with an active-area of 0.25 cm^2 defined by the top Indium-Tin-Oxide were measured under an AM1.5 solar simulator at 25 ˚C. In order to characterize long wavelength performance, the J-V characteristics were also measured with 610-nm and 630-nm long-pass filters for the middle and bottom cells, respectively. Quantum efficiency (QE) curves were measured under the short-circuit condition with no optical bias. The short-circuit current density (J_{sc}) values were calculated by integral of the QE data with the AM1.5 spectrum.

Similar to previously reported [2], the J_{sc} increases with the surface roughness (RMS as well the correlation length) of the substrates. As shown in Fig. 4, the surface roughness is saturated when the ZnO film thickness is over 2 μm. Therefore, we mainly compared the back reflectors of a ZnO thickness of 2 μm. The Ag/ZnO back

Table II. J-V characteristics of a-SiGe:H bottom cells made on three different Ag/ZnO back reflectors. The J_{sc} were calculated from the integral of QE curves with AM1.5 spectrum in the wavelength range of 630 nm to 1000 nm and the V_{oc} and FF from J-V measurements under an AM1.5 solar simulator with a 630-nm long-pass filter.

Sample #	Substrate	J_{sc} (mA/cm^2)	V_{oc} (V)	FF	P_{max} (mW/cm^2)
16147	R1938	9.98	0.634	0.612	3.87
16124	R1938	10.38	0.635	0.581	3.83
16135	R8342	10.69	0.643	0.628	4.32
16142	R8345	11.30	0.641	0.607	4.37
16146	R8345	10.94	0.638	0.582	4.06

Table III. J-V characteristics of a-SiGe:H middle cells made on three different Ag/ZnO back reflectors. The J_{sc} were calculated from the integral of QE curves with AM1.5 spectrum in the wavelength range of 610 nm to 1000 nm and the V_{oc} and FF from J-V measurements under an AM1.5 solar simulator with a 610-nm long-pass filter.

Sample #	Substrate	J_{sc} (mA/cm^2)	V_{oc} (V)	FF	P_{max} (mW/cm^2)
16130	R1938	10.18	0.734	0.634	4.74
16136	R1938	9.72	0.740	0.635	4.67
16138	R8342	10.61	0.740	0.648	5.09
16141	R8345	10.88	0.745	0.627	5.08

reflector (R1938) from the 5MW machine was used as a baseline. Two other Ag/ZnO back reflectors were selected for comparison. R8342 has a flat Ag layer and a textured ZnO layer with a thickness of 2 μm. R8345 is the same as R8342 except a textured Ag layer. Tables II and III list the J-V characteristics of the a-SiGe:H middle and bottom cells, respectively. In each type of cells, two baseline samples were included to indicate the run-to-run variations.

From the two tables, one can see that the thicker ZnO layer with a large roughness indeed enhances the long wavelength current. Comparing the performance of cells having a flat Ag (R8342) layer with those having a textured Ag (R8345), we found that the textured Ag still produces more current than the flat Ag as shown in Fig. 7, although the total absorption might be high at the textured interface between the Ag and ZnO layers due to extra plasmon absorption. Actually, the textured Ag has two effects on the light trapping. The positive effect is the textured interface between the Ag and ZnO layers produce more scattered light, especially for a thin ZnO layer; the negative effect is that the extra area resulting from the textured interface causes more plasmon absorption and extra loss could be caused by some deep valleys. These two competing factors determine the total light trapping effect. Under the current conditions, the textured Ag layer still produces more current than the flat Ag layer.

1. 4. Summary

We have carried out a systematic study on Ag/ZnO structures with the collaboration of NREL. The XRD measurements show that the Ag and ZnO layers have a (111) and (002) preferential crystal orientation, respectively. Two surprising phenomena are observed. First, both the flat and textured Ag layers have a similar grain size. Second, the ZnO grain size does not show a tendency of growth with film thickness. The AFM measurements show that both the RMS roughness and surface correlation length increase with the ZnO layer thickness. The RMS roughness saturates for the ZnO layer thicker than 2 μm.

We have used a-SiGe:H middle and bottom cells to qualify the Ag/ZnO back reflectors and found that a back reflector with a textured Ag and a thicker ZnO gives the highest current. Although a flat Ag layer might reduce the loss in the Ag/ZnO interface region, a textured Ag might enhance the light scattering.

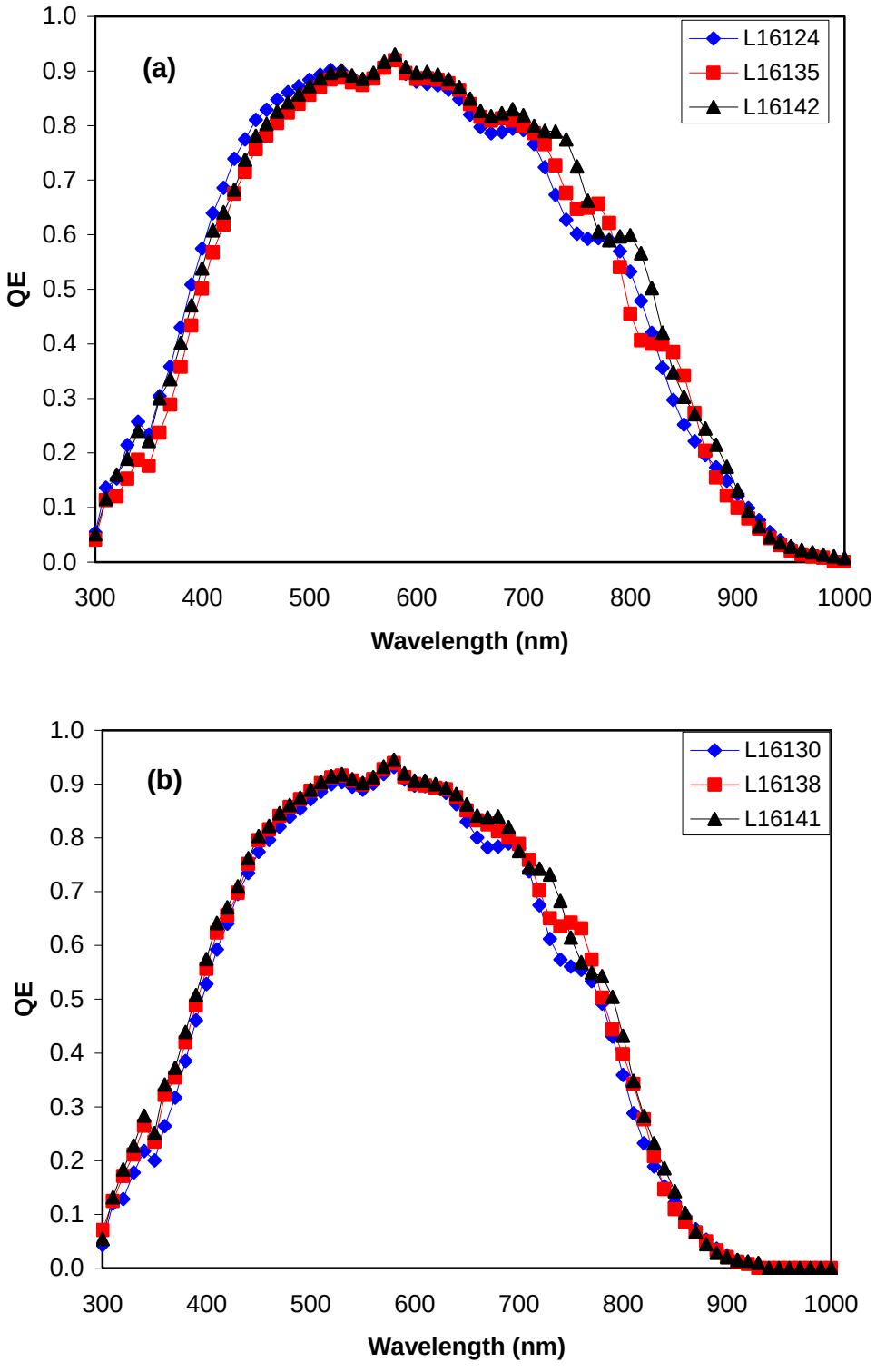

Figure 7. QE curves of a-SiGe:H (a) bottom and (b) middle cells on different Ag/ZnO back reflectors as listed in Tables II and III.

2. Stability study of double-junction solar cells under different electric bias

2. 1. Introduction

It is well known that light-induced defect generation leads to the degradation of a-Si:H-based material quality and solar cell performance. Although no convincing explanation of the light-induced degradation has been accepted, it is generally believed that the light-induced defect creation is caused by recombination of excess electron-hole pairs generated by photoexcitation or forward-bias current injection. Applying a reverse bias to an a-Si:H solar cell during light-soaking reduces the recombination probability of the electron-hole pairs, and hence reduces the light-induced degradation in a-Si:H based solar cells.

On the other hand, the light-induced metastability in nc-Si:H solar cells is different from that in a-Si:H solar cells [8-10]. Previously, we found that there was no current-induced degradation under forward bias, but an enhanced light-induced degradation under reverse bias in nc-Si:H cells. The reverse-biased enhanced light-induced degradation increases with the increase of reverse bias magnitude. Based on the nature of the nc-Si:H material structure, we proposed a back-to-back diode model to explain the observed phenomenon.

The stability behavior of a-Si:H/nc-Si:H double junction solar cells under the open circuit condition has been investigated extensively. Because nc-Si:H cells are stable under red light, an a-Si:H/nc-Si:H double-junction cell with a bottom cell limited current mismatch is desirable to obtain a high stabilized efficiency. However, in the real application, the solar cells may be subjected to different bias conditions. Further, each component cell may work under different biases, depending on the current mismatch under a given illumination. For example, under short circuit condition, if an a-Si:H/nc-Si:H double-junction cell has a bottom cell limited current mismatch, the nc-Si:H bottom cell works under a reverse bias. However, if the a-Si:H/nc-Si:H double-junction solar cell has a top cell limited current mismatch, the a-Si:H top cell works under the reverse bias condition. Obviously, light-soaking behavior of a-Si:H/nc-Si:H double-junction cells under different electric bias conditions might be different. In this quarter, we have studied the electric bias effect on the a-Si:H/nc-Si:H double-junction solar cells.

2. 2. Experimental details and results

Two particular a-Si:H/nc-Si:H double junction samples were made, in which the a-Si:H top cell recipe was kept the same. One has a strong bottom cell limited current, and the other has strong top cell limited current. The different current mismatches were achieved by varying the nc-Si:H bottom cell thickness. For each experiment, three cells on the same substrate were selected for light soaking simultaneously. One cell was shorted during the light soaking, which corresponds to a zero bias condition. A forward bias with a value at the maximum power was applied to the second cell. The third cell was light-soaked under the open circuit condition, which is equivalent to a forward bias with a value of V_{oc}. The light soaking was carried out under 100 mW/cm^2 white light at

50°C for one week. Then, the light-soaked samples were annealed under vacuum at 150°C for 2 hours to check the reversibility of the light-induced degradation.

Table IV lists the light-soaking results for the a-Si:H/nc-Si:H double-junction cells with a strong bottom cell limited current. The QE measurements showed that the top cell is able to provide a current density of 11.4 mA/cm^2, while the bottom cell current density is around 9.7-10.8 mA/cm^2, depending on the cell location. FF_r and FF_b are the fill factors obtained from J-V measurements under the AM1.5 solar simulator with a 610-nm long-pass filter (red light) and a 585-nm short-pass filter (blue light), respectively. Under the red light, the cell performance is strongly limited by the top cell due to a small amount of absorption in the a-Si:H intrinsic layer. Similarly, under the blue light, the cell performance is limited by the bottom cell. Therefore, the FF_r is a measure of the top cell performance, and FF_b reflects the bottom cell performance. From Table IV, one can see that under the short circuit condition, the cell efficiency degraded by 27.7%, which is the highest degradation in three bias conditions. Such a high light-induced degradation may also partially results from the relatively poorer initial performance and the larger current mismatche than other two cells. Under the open circuit condition, the degradation of the cell efficiency is ~10.3% and it is the smallest among the three cells. The degradation of 12.6% under the forward bias at maximum power is in between the short circuit and open circuit conditions. From the FF_r and FF_b measurements, we found that the change in the FF_r was very similar for the three cells, whereas the FF_b changes were dramatically different under different bias voltages. The FF_b decreased by 13.5% under the short circuit condition, and showed no change under the open circuit condition with experimental error. Clearly, the highest light-induced degradation in the efficiency of the a-Si:H/nc-Si:H double-junction cell under the short circuit condition resulted from the extra degradation in the bottom cell.

Table V lists the light-soaking results of the a-Si:H/nc-Si:H double junction cells with a strong top cell limited current. QE measurements show that the top cell has a current density of ~10.7 mA/cm^2, and bottom cell of ~13.2 mA/cm^2. Although top cell has the same recipe as sample 15299 in Table IV, the current density is smaller. This is because the top cell receives less benefit from back reflector due to the thicker bottom cell. The light-soaking results in Table V are different from those in Table IV. The cell with a strong top cell limited current mismatch under the short circuit condition has the smallest light-induced degradation. The degradation increases with increasing the forward bias. The FF_r also showed the similar trend, which means that the degradation was mainly in the a-Si:H top cells. For comparison, the efficiency degradation as a function of the electrical bias for two types of a-Si:H/nc-Si:H cells with different current mismatches is plotted in Fig. 8. The samples were annealed in vacuum after the light-soaking, and the cell performances were recovered as shown in Tables IV and V.

For understanding the mechanisms of the different behaviors of electrical bias dependence of a-Si:H/nc-Si:H double junction solar cells with different current mismatches, Fig. 9 plots the decomposed J-V curves of the component cells in the two types of a-Si:H/nc-Si:H double junction solar cells. In Fig. 9 (a), the double junction cell has a bottom cell limited current. Under the short circuit condition, the top cell works under the forward bias at point A. To compensate for this voltage, the bottom cell works under the reverse bias at point B, which means the nc-Si:H bottom cell is reversely biased during light-soaking. From previous studies [8-10], we learned that the reversely biased

Table IV. Light-induced degradation of a-Si:H/nc-Si:H double-junction solar cells with a strong bottom cell limited current mismatch under different bias conditions. The forward bias value is close the maximum power. The light soaking was done under 100 mW/cm^2 white light at 50 ^{o}C for 1 week (168 hours).

Cell No.	Bias Condition	Status	V_{oc} (V)	FF			Q (mA/cm^2)			P_{max} (mW/cm^2)
				AM1.5	FF_r	FF_b	Q(total)	Q(top)	Q(bottom)	
42	Short circuit (0 V)	Initial	1.409	0.709	0.746	0.773	21.15	11.43	9.72	9.71
		Light-soaking	1.361	0.582	0.677	0.669	19.85	10.99	8.86	7.02
		Degradation	3.4%	17.9%	9.2%	13.5%	6.1%	3.8%	8.8%	27.7%
		Annealed	1.399	0.726	0.741	0.801	20.64	11.13	9.51	9.66
22	Forward bias (+1.13 V)	Initial	1.434	0.735	0.759	0.809	21.97	11.41	10.56	11.13
		Light-soaking	1.408	0.682	0.688	0.795	21.16	11.03	10.13	9.73
		Degradation	1.8%	7.2%	9.4%	1.7%	3.7%	3.3%	4.1%	12.6%
		Annealed	1.453	0.739	0.752	0.816	21.36	11.10	10.26	11.02
32	Open circuit (+1.43 V)	Initial	1.429	0.735	0.741	0.778	22.20	11.38	10.82	11.36
		Light-soaking	1.403	0.686	0.681	0.792	21.53	10.94	10.59	10.19
		Degradation	1.8%	6.7%	8.1%	0	3.0%	3.9%	2.1%	10.3%
		Annealed	1.450	0.735	0.751	0.805	21.64	11.05	10.59	11.29

Table V. Light-induced degradation of an a-Si:H/nc-Si:H double-junction solar cell with a strong top cell limited current under different bias conditions. The forward bias value is the voltage at maximum power. The light-soaking was done under 100 mW/cm^2 white light at 50 ^{o}C for 1 week (170 hours). The sample No. is RF 15300.

Cell No.	Bias Condition	Status	V_{oc} (V)	FF			Q (mA/cm^2)			P_{max} (mW/cm^2)
				AM1.5	FF_r	FF_b	Q(total)	Q(top)	Q(bottom)	
23	Short circuit (0 V)	Initial	1.521	0.701	0.763	0.781	23.81	10.67	13.14	11.38
		Light-soaking	1.498	0.656	0.711	0.775	23.49	10.41	13.08	10.23
		Degradation	1.5%	6.4%	6.8%	0.77%	1.3%	2.4%	0.5%	10.1%
		Annealed	1.532	0.702	0.763	0.788	23.26	10.42	12.84	11.21
22	Forward bias (+1.20 V)	Initial	1.515	0.712	0.762	0.789	23.92	10.74	13.18	11.59
		Light-soaking	1.490	0.662	0.704	0.777	23.52	10.41	13.10	10.27
		Degradation	1.7%	7.0%	7.6%	1.5%	1.7%	3.1%	0.6%	11.4%
		Annealed	1.527	0.702	0.762	0.790	23.53	10.54	12.99	11.30
32	Open circuit (+1.51 V)	Initial	1.506	0.693	0.765	0.781	24.05	10.81	13.23	11.28
		Light-soaking	1.477	0.644	0.688	0.779	23.49	10.45	13.04	9.94
		Degradation	1.9%	7.1%	10.1%	0.3%	2.3%	3.3%	1.4%	11.9%
		Annealed	1.518	0.693	0.755	0.781	23.50	10.55	12.95	11.10

nc-Si:H bottom cell should show an enhanced degradation, which is in agreement with the experimental results shown in Table IV. We also need to point out that the degradation in the bottom cell depends on the top cell thickness. If the top cell is thick enough so that no high energy photons (energy larger than the bandgap of the amorphous phase in the nc-Si:H intrinsic layer) can reach the nc-Si:H bottom cell, the nc-Si:H bottom cell is not expected to be degraded even if an reverse bias is applied to the bottom cell.

For the top cell limited a-Si:H/nc-Si:H double-junction cell as described in Fig. 9 (b), under the short circuit condition, the bottom cell is under forward bias at point A, and the top cell is under reverse bias at point B. The reverse bias reduces light-induced degradation in an a-Si:H solar cell. Under the open circuit condition, both component cells also work under open circuit condition. Thus, the top cell has a big degradation. This is also consistent with the experimental results in Table V.

2. 3. Summary

In summary, we have systematically studied the electrical bias effect on the light-induced degradation in a-Si:H/nc-Si:H double-junction solar cells. Three electrical bias conditions were used: the short-circuit, the maximum power, and the open circuit. We found that the light-soaking behaviors under different electrical biases are different for the a-Si:H/nc-Si:H double-junction solar cells with different current mismatches. Under the short circuit condition, the a-Si:H/nc-Si:H double-junction cells with a bottom cell limited current mismatch showed the highest degradation, whereas the cell with a top cell limited current has the smallest degradation. Because the electrical bias dependence of stability is different in a-Si:H/nc-Si:H double-junction solar cells from conventional a-Si:H/a-SiGe:H/a-SiGe:H triple-junction solar cells, one might take this effect into consideration for solar energy system design.

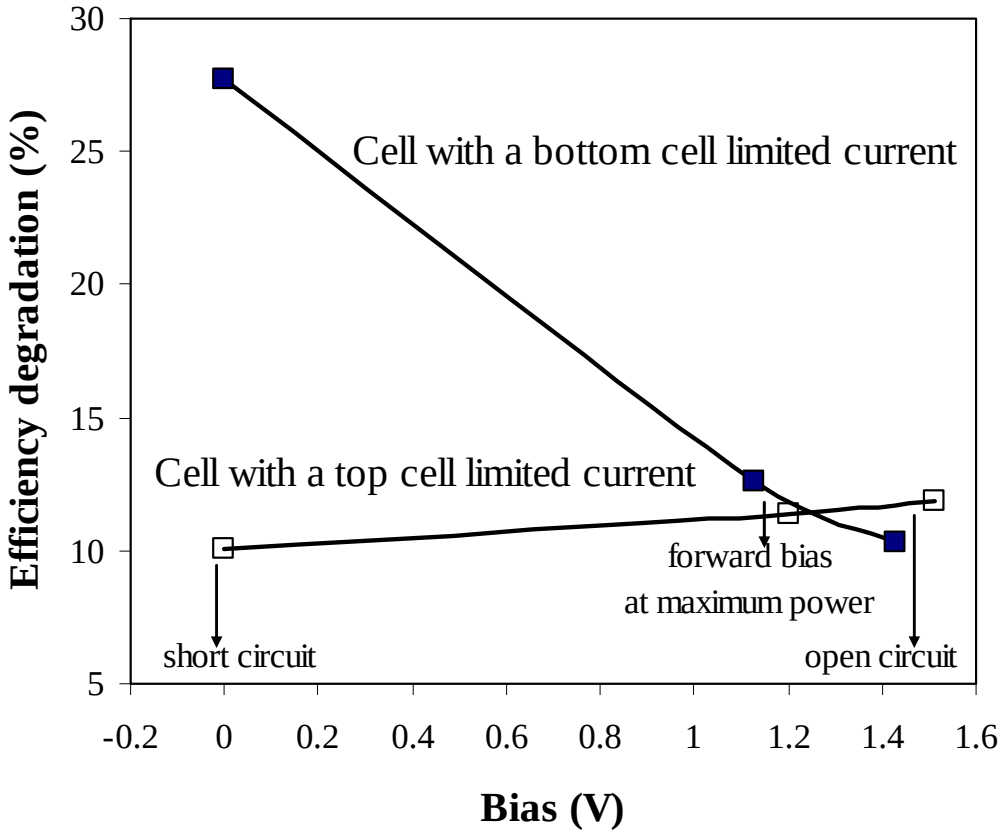

Figure 8. Light-induced degradation in the efficiency of a-Si:H/nc-Si:H double-junction solar cells as a function of electrical bias during the light soaking. The two types of a-Si:H/nc-Si:H double-junction solar cells have different current mismatches.

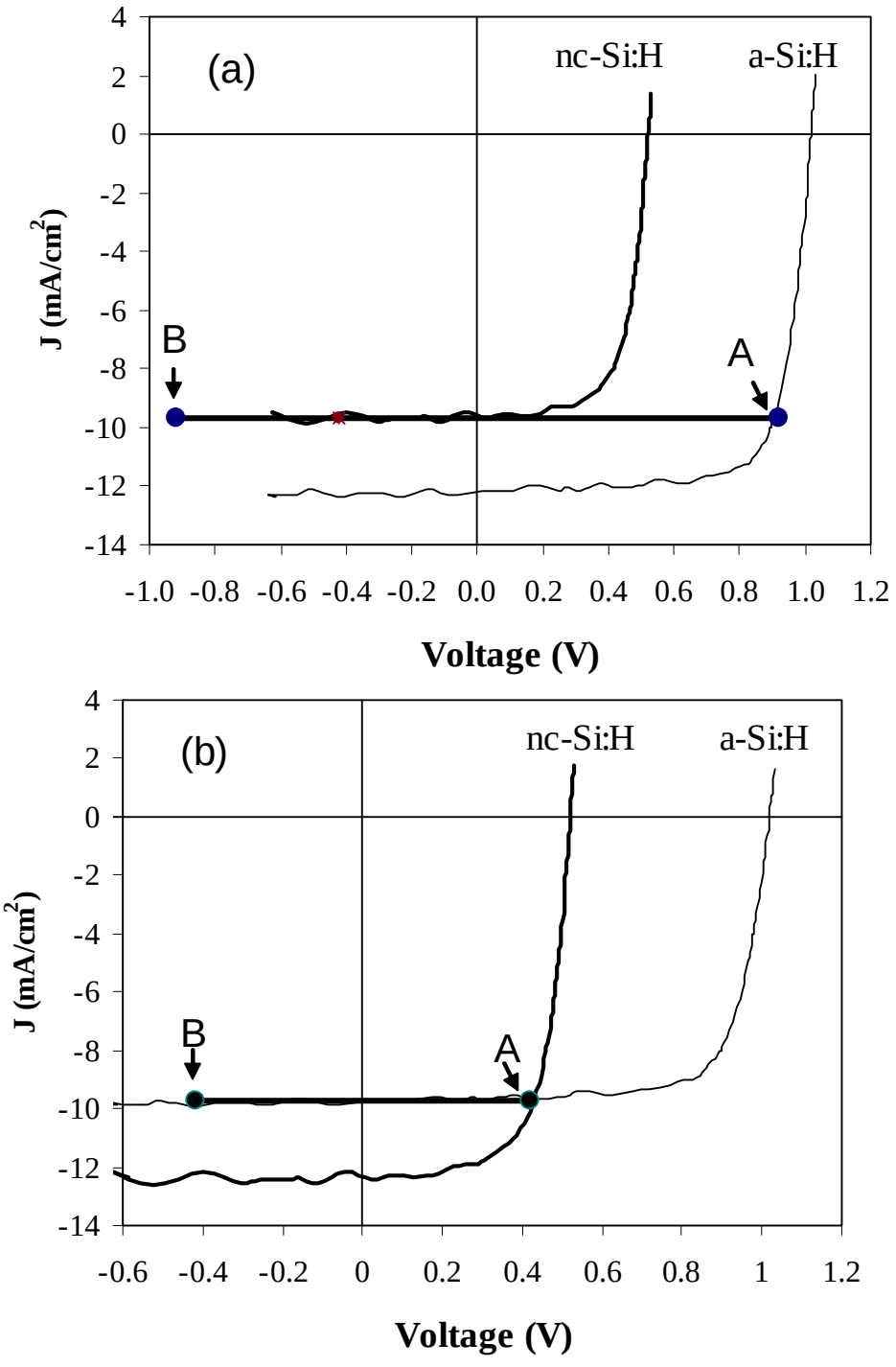

Figure 9. Illustration of J-V curves of the component cells in a-Si:H/nc-Si:H double-junction solar cells with (a) a bottom cell limited current, and (b) a top cell limited current mismatches.

3. Large-area a-Si:H/nc-Si:H double-junction modules

We have continued to work on large-area a-Si:H/nc-Si:H double-junction cells using one of our large area multi-chamber batch system (2B) using RF glow discharge decomposition of SiH_4 diluted with H_2. In this quarter, the effort has been mainly focused on optimizing processing parameters under a lower pressure and a larger spacing between the cathode and sample substrate, which may ease process control in large volume manufacturing. The preliminary results are summarized in Table VI, which show that the cell performance made with the new processing conditions is comparable to the best cell performance achieved at the higher pressure and narrower spacing [11]. The processing parameters are still under the optimization, and new results will be presented in the next report.

Table VI. J-V characteristics of newly made a-Si:H/nc-Si:H double-junction solar cells (first two rows). The cells (last two rows) previously made with higher pressure and narrower spacing are also listed for the comparison [11].

Sample No.	Area (cm^2)	V_{oc} (V)	FF	J_{sc} (mA/cm^2)	Eff. (%)	Comment
2B11770	462	1.48	0.762	10.40	11.73	Wider spacing
2B11774	462	1.49	0.743	10.53	11.66	
2B10582	420	1.44	0.729	11.21	11.77	Narrow spacing
2B10587	420	1.44	0.689	11.68	11.59	

References:

1. A. Banerjee and S. Guha, J. Appl. Phys. **69**, 1030 (1991).
2. B. Yan, G. Yue, J.M. Owens, J. Yang, and S. Guha, Conf. Record of the 2006 IEEE 4th World Conf. on Photovoltaic Energy Conversion, (Hawaii, USA, May 7-12, 2006), p. 1477.
3. G. Yue, B. Yan, G. Ganguly, J. Yang, S. Guha, C. Teplin, and D. L. Williamson, Conf. Record of the 2006 IEEE 4th World Conf. on Photovoltaic Energy Conversion, (Hawaii, USA, May 7-12, 2006), p. 1588.
4. J. Yang, A. Banerjee, and S. Guha, Appl. Phys. Lett. **70**, 2975 (1997).
5. B. Yan, J. M. Owens, C.-S. Jiang, J. Yang, and S. Guha, *Mater. Res. Soc. Symp. Proc.* **862**, A23.3 (2005).
6. P. B. Barrna and M. Adamik, Thin Films **317**, 27 (1998).
7. J. A. Thornton, J. Vac. Sci. Tech. **A4**, 3059 (1986).
8. G. Yue, B. Yan, J. Yang, and S. Guha, Appl. Phys. Lett. **86,** 092103 (2005).
9. G. Yue, B. Yan, J. Yang, and S. Guha, J. Appl. Phys. **98**, 074902 (2005).
10. G. Yue, B. Yan, G. Ganguly, J. Yang, and S. Guha, Appl. Phys. Lett. **88**, 263507 (2006).
11. S. Guha and J. Yang, Final technical progress report of the Thin Film Partnership program Subcontract No. ZDJ-2-30630-19, p.86